Structural Feature and Catalytic Performance of Cu Species Distributed over TiO_2 Nanotubes

Jun-Nan Nian, Shin-An Chen, Chien-Cheng Tsai, and Hsisheng Teng*

Department of Chemical Engineering, National Cheng Kung University, Tainan 70101, Taiwan

Received: July 5, 2006; In Final Form: October 14, 2006

Copper oxide was deposited on tubular TiO_2 via Cu^{2+} introduction into a titanate nanotube aggregate followed by calcination. The titanate has a layered structure allowing Cu intercalation and can readily transform into anatase TiO_2 via calcination for condensation of the constituting layers. The activity of the tubular catalysts, with a Cu content of 2 wt %, in selective NO reduction with NH_3 was compared with those of other 2 wt % Cu/TiO_2 catalysts using TiO_2 nanoparticles as the support. The Cu species supported on the nanotubes showed a higher activity than those supported on the nanoparticles. X-ray absorption near-edge structure (XANES) analysis showed that the Cu species on all the TiO_2 supports are in the +2 state. Extended X-ray absorption fine structure (EXAFS) investigations of these catalysts reflected higher degrees of CuO dispersion and Cu^{2+} dissolution into the TiO_2 lattice for the tubular Cu/TiO_2 catalysts. Absence of CuO bulk detection by a temperature-programmed reduction analysis for the tubular catalysts confirmed the high CuO-dispersion feature of the tubular catalysts. The dissolution of Cu^{2+} to form a $Cu_xTi_{1-x}O_2$ type of solid solution was improved by using an in-situ ion-intercalation method for Cu deposition on the nanotubes. A fraction as high as 40% for Cu^{2+} dissolution was obtained for the tubular catalysts while only 20% was obtained for the particulate catalysts. The $Cu_xTi_{1-x}O_2$ species were considered one form of the active sites on the Cu/TiO_2 catalysts.

Introduction

TiO_2, which is chemically stable but active in promoting catalytic effects, has been used as a support for metal-oxide catalysts in many reactions including oxidation of CO and hydrocarbons and selective catalytic reduction (SCR) of NO because of the high activity of the supported species at relatively low temperatures.[1−4] For a support, a large surface area is the essential feature to disperse the active species.[5] In addition, the microstructure or morphology of the support framework or the method by which the active species is introduced affects not only the dispersion but also the structure and chemical environment of the active species.[6] In the present work, we intended to explore the possibility using titanate-derived TiO_2 nanotubes to improve the metal-oxide dispersion over TiO_2 and thus the activity of the resulting catalysts.

Titanate-based nanotube aggregates prepared from hydrothermal treatment on TiO_2 in alkali solutions have been shown to possess a large surface area.[7−10] Upon mild calcination (<400 °C), the nanotubes exhibit a well-defined phase of the anatase TiO_2 while still retaining the tubular structure.[8d] The titanate nanotubes are believed to form through scrolling the sheets peeled off from the titanate matter.[9b,d] This leads to a multilayer feature for the tube wall. By using this titanate nanotube aggregate as a support, it is expected that the layered structure would provide sites for the intercalation of metal ions,[9c] thus assisting in accommodation of the active species as well as preventing agglomeration of the species in the subsequent calcination for phase transformation into anatase TiO_2. The highly dispersed metal oxide over a support is believed to be the active phase for heterogeneous catalysis.[11] A high capacity and even distribution for ruthenium ions over this tubular titanate have been reported.[2c]

In the present study, we used copper oxides as the active species to explore the capability of the nanotubes in improving the dispersion of active metal oxides and thus the resulting activity, which was examined with SCR of NO. Copper oxides supported on different porous materials are active in catalyzing selective NO reduction in the presence of O_2,[4,11−14] although their stability is one of the important challenges. We extensively studied the dispersion, as well as the coordination with the TiO_2 support, of the Cu species with X-ray absorption fine structure spectroscopy and other techniques, attempting to give correlations between the structural feature of Cu species and the catalytic activity. Here, we report the structure of Cu species supported on titanate-derived TiO_2 nantubes and commercially available TiO_2 nanoparticles and show that the Cu species supported on the nanotubes are more highly dispersed and dissolved into TiO_2 and are more active in catalyzing NO reduction.

Experimental Section

Synthesis. The nanotube TiO_2 aggregates were synthesized by using a commercially available P25 TiO_2 (Degussa, Germany; surface area = 50 m^2/g) as the precursor. The preparation was analogous to those previously reported.[7,10e] P25 (3 g) was hydrothermally treated with 10 N NaOH (100 mL) in a Teflon-lined autoclave at 130 °C for 24 h. The slurry, which contained a titanate composed of lamellar layers,[9,10] was then washed with 0.1 N HCl solution (1 L) for several times to reach a pH value of 1.6. After filtration, the obtained solid was dried at 110 °C for 12 h to give the nanotubes.

The nanoparticle TiO_2 supports used in the present study were P25 and other commercially available large-surface-area prod-

* Author to whom correspondence should be addressed. Tel: 886-6-2385371; fax: 886-6-2344496; e-mail: hteng@mail.ncku.edu.tw.

10.1021/jp064209w CCC: $33.50
Published on Web 11/30/2006

ucts, UV100 (Sachtleben, Germany; surface area = 340 m^2/g) and ST01 (Ishihara, Japan; surface area = 320 m^2/g). These large-surface-area products had average particle sizes less than 10 nm.

The introduction of Cu into the tubular or particulate TiO_2 aggregates was conducted by using incipient-wetness impregnation of $Cu(NO_3)_2$ with stirring and sonication at the ambient temperature and then vacuum drying at 110 °C for 12 h. The concentration of $Cu(NO_3)_2$ solutions was adjusted to prepare catalysts of 2 wt % Cu-loading, which was also confirmed with atomic absorption spectrometry. Calcination of the Cu-loaded specimens at 400 °C for 1 h was conducted to give the final Cu-loaded catalysts for further analysis and examination. The catalysts were designated as Cu/NT for Cu supported on the nanotubes and Cu/P25, Cu/UV, and Cu/ST for Cu supported on the P25, UV100, and ST01 nanoparticles, respectively. Taking advantage of the layered structure of the titanate species, the degree of Cu dispersion over the nanotubes is expected to be improved by carrying out an in-situ Cu-incorporation during the period of titanate nanotube formation. To prepare this type of Cu-loaded nanotubes, an appropriate amount of $Cu(NO_3)_2$ was added to the TiO_2/NaOH mixture for the hydrothermal treatment, which was also followed by the HCl washing for nanotube formation. After vacuum drying at 110 °C for 12 h, the Cu-loaded nanotube specimen was also calcined at 400 °C for 1 h to give the final catalyst (Cu/NT1; 2 wt % in Cu).

Characterization. The phase identification of the specimens was conducted with powder X-ray diffraction (XRD) using a Rigaku RINT2000 diffractometer equipped with Cu Kα radiation. The data were collected for scattering angles (2θ) ranging between 5 and 70° with a step size of 0.01°. The microstructures were explored with a transmission electron microscope (TEM; Hitachi FE-2000, Japan). The Brunauer−Emmett−Teller surface areas of the samples were determined by N_2 adsorption at −196 °C using an adsorption apparatus (Micromeritics ASAP 2010, United States). The amount of N_2 adsorbed at relative pressures near unity ($p/p_0 = 0.96$ here) was used to give the total pore volume. The average pore diameter was determined from the surface area and pore volume, under the assumption of cylindrical-pore configuration.[15]

Structural feature and chemical environment of the Cu species on the supports were characterized by X-ray absorption fine structure spectroscopy, including X-ray absorption near-edge structure (XANES) and extended X-ray absorption fine structure (EXAFS). The spectra were measured on the Wiggler beam line of the Taiwan Synchrotron Radiation Research Center. A double-crystal Si(111) was used to monochromatize X-rays from the 1.5 GeV electron storage ring with a current range of 120−200 mA. Photon energy was calibrated by characteristic preedge peaks in the absorption spectrum of Cu foil (8979 eV). The EXAFS data were analyzed using the UWX-AFS 3.0 and FEFF 7.0 programs.[16] Fourier transformation was performed on k^3-weighted EXAFS oscillation in the range of 2.8−14 $Å^{-1}$. Multiple shell fitting of the EXAFS data was conducted in the R-space.

Catalytic Measurement. Selective reduction of NO with NH_3 was performed over a catalyst bed packed within a Pyrex tube with 1 cm in diameter. The fixed bed consisted of 0.2-g catalyst particles with a type K thermocouple placed at the center of the bed for temperature measurements. Reactant gases (640 ppm NO, 640 ppm NH_3, and 1 vol % O_2) were fed to the reactor through mass flow controllers, and helium was added to make up a total flow rate of 300 cm^3/min. The gas hourly space velocity (GHSV) was about 10 000/h for this system. The NO reduction experiments were conducted at temperatures ranging between 100 and 350 °C. The NO concentration was analyzed by a chemiluminescence NO/NO_x analyzer. Gas chromatography (Hewlett-Packard HP6890, United States; molecular sieve 5A column, TCD, He carrier) was used to analyze the product stream, which was principally comprised of NO, NH_3, O_2, N_2, and H_2O. Nitrogen was found to be the main product of NO reduction in the present work, and only negligible amounts of N_2O and NO_2 can be detected

The surface reducibility of the catalysts was studied by temperature-programmed reduction (TPR). Prior to each TPR experiment, the catalyst was pretreated in O_2 at 400 °C for 1 h. TPR was carried out under a flow of 10 vol % H_2/He mixture from room temperature to 750 °C at a heating rate of 10 °C/min. A thermal conductivity detector was used to continuously monitor the consumption of H_2 during the TPR. The volume of hydrogen taken up by the catalysts was calibrated against pure CuO. The decomposition of the experimental convoluted TPR peaks was performed by using a nonlinear least-squares fitting program with a symmetric Gaussian function.

Results and Discussion

Figure 1 shows the TEM images of the specimens derived from the consecutive treatments, including the hydrothermal autoclaving, the posttreatment acid washing, and finally the calcination at 400 °C, on the P25 TiO_2 precursor for synthesis of nanotube aggregates. The corresponding XRD patterns are depicted in Figure 2. After the hydrothermal treatment in NaOH, the TiO_2 precursor transformed into titanate, as indicated by the XRD pattern in Figure 2a. This titanate material obtained from the hydrothermal treatment in NaOH was suggested to be $Na_{2-x}H_xTi_2O_5 \cdot H_2O$ because its diffraction pattern was consistent with that of $H_2Ti_2O_5 \cdot H_2O$ (bottom of Figure 2) documented in the powder diffraction files of the Joint Committee on Powder Diffraction Standards.[17] The TEM image of this titanate in Figure 1a shows a condensed phase containing multilayered structure, which is characteristic of $H_2Ti_2O_5 \cdot H_2O$.[17] Upon acid washing, the titanate sheets would peel off and scroll into tubes,[9d] accompanied by Na^+ substitution with proton.[10a,e] However, after the acid washing to reach a pH of 1.6, the material not only transformed to a tubular configuration (Figure 1b) but also showed a dramatic change in the crystalline structure from the titanate to a hybrid of the titanate and anatase TiO_2 (Figure 2b). The XRD pattern shows an obvious weakening of the peaks at $2\theta = 9.2$, 24, and 28°, which respectively correspond to the characteristic diffraction of (200), (110), and (310) faces of the titanate, while the anatase TiO_2(101) diffraction at $2\theta = 25°$ can be seen to show up. The readiness of this phase transition from the titanate to anatase TiO_2 was attributed to the fact that both phases own a zigzag arrangement for their constituting TiO_6-octahedron layers (top of Figure 2).[10e,f] After calcining the nanotubes at 400 °C, the tubular structure shrank and was damaged (Figure 1c), although the contour of the tubular framework seemingly remained. The TEM image of the Cu-containing tubular TiO_2 (see Supporting Information) was similar to that shown in Figure 1c. The well-defined anatase phase is exclusively present in the XRD pattern of the calcined specimen (Figure 2c), however. The calcination may have caused dehydration of the layered titanate on the walls into anatase TiO_2, thus leading to the rupture of the tubular structure.

The physical characteristics of the TiO_2 supports determined from N_2 adsorption are summarized in Table 1. The surface areas of UV100, ST01, and NT are large (>300 m^2/g), except that of P25. The pore volume of the commercially available

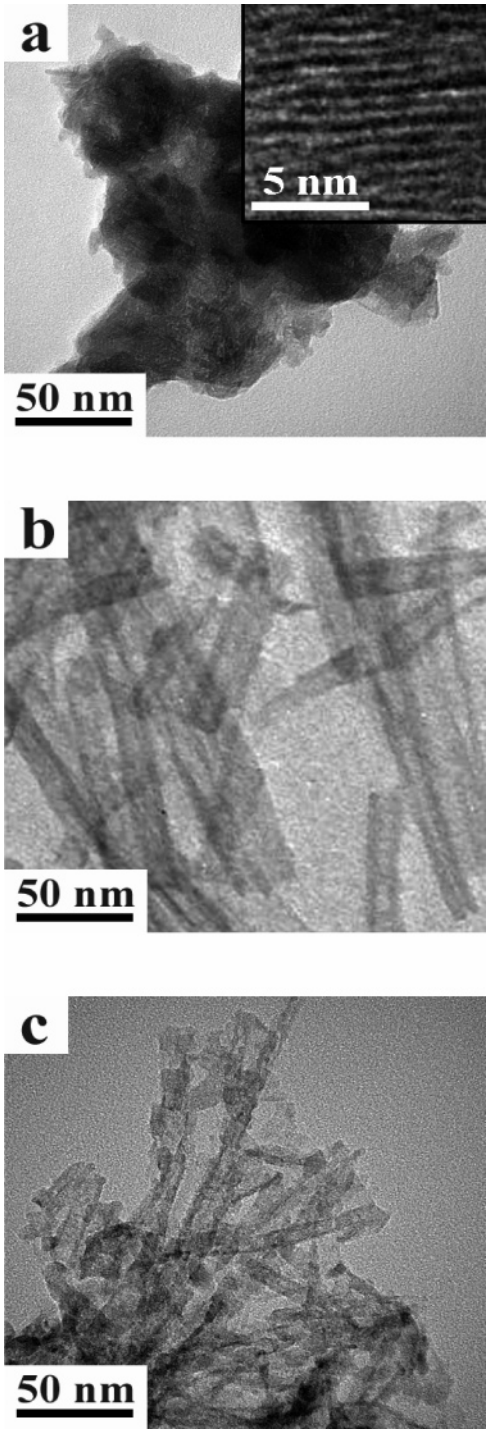

Figure 1. TEM images of the specimens obtained after the consecutive treatments on the P25 TiO_2 precursor: the hydrothermal autoclaving in NaOH (a), the posttreatment acid washing (b), and finally the calcination at 400 °C (c).

samples is mainly contributed by the interstices between the nanoparticles. The pore size, which corresponds to the interstice width, would increase with the size of the constituting nanoparticles. Accordingly, an order of P25 > ST01 > UV100 for the particle size is thus expected. The pore volume of the nanotubes, on the other hand, is contributed by the internal volume inside the tubes as well as the interstices between the tubes. This large-surface-area feature for these TiO_2 materials is advantageous for dispersion of active species.

All the Cu-loaded catalysts prepared from the $Cu(NO_3)_2$ impregnation had been calcined at 400 °C to remove the nitrate

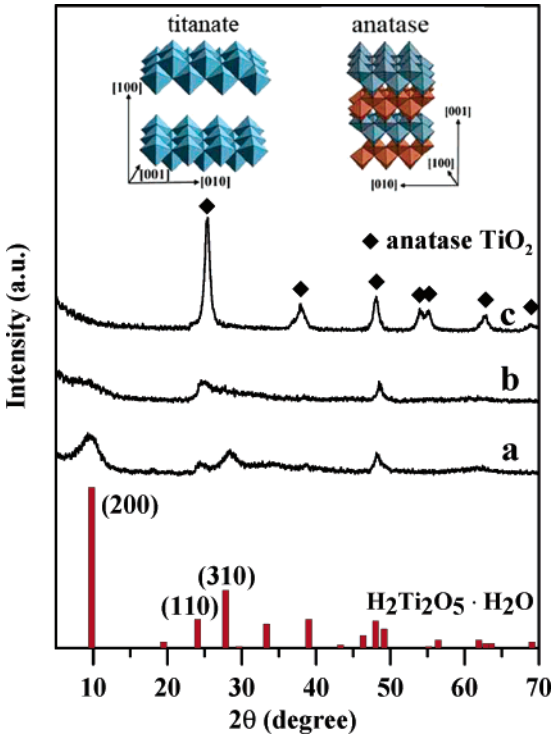

Figure 2. Powder XRD patterns of the specimens obtained after the consecutive treatments on the P25 TiO_2 precursor: the hydrothermal autoclaving in NaOH (a), the posttreatment acid washing (b), and finally the calcination at 400 °C (c).

TABLE 1: The Physical Characteristics of the TiO_2 Supports

samples	*surface area* (m^2/g)	*pore volume* (cm^3/g)	*average pore* diameter (nm)
P25	50	0.13	14
UV100	340	0.35	5.6
ST01	320	0.60	7.4
NT	390	1.2	12

and to minimize the possible textural variation during the SCR experiments, which were conducted at 100−350 °C. Because the calcination caused agglomeration of the TiO_2 supports, Cu/UV, Cu/ST, and Cu/NT showed surface areas of ca. 100, 110, and 190 m^2/g, respectively, and pore volumes of ca. 0.25, 0.54, and 0.86 cm^3/g. Supported active oxides generally sinter upon thermal treatment. However, no copper oxide peaks can be observed in the XRD patterns of the Cu/TiO_2 catalysts shown in Figure 3. This indicates that Cu species were well-dispersed to a certain extent and that the crystalline size of copper oxides was too small to be detected by the diffraction. Only the anatase TiO_2 phase can be detected by XRD for all the Cu/TiO_2 catalysts shown in Figure 3. As to the Cu/P25 catalysts, catalytic measurements showed that Cu/P25 exhibited a relatively low SCR activity (Figure 4), and its structure was not further explored in the following discussion.

The catalysts from the incipient-wetness impregnation, Cu/ST, Cu/UV, and Cu/NT, were all subjected to activity analysis with the SCR reaction. The temperature dependence of the steady-state NO conversion with NH_3 over the Cu/TiO_2 catalysts is shown in Figure 4. Preliminary experiments have revealed that the activity of all the bare TiO_2 supports in NO reduction was negligibly low, and the data are not presented. The activity increased significantly upon Cu loading. Figure 4 shows that, for these catalysts with 2 wt % Cu content, a conversion maximum can be reached at temperatures of ca. 300 °C and

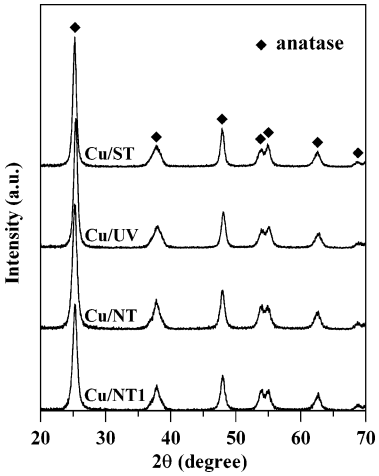

Figure 3. Powder XRD patterns of the Cu-loaded (2 wt %) TiO_2 catalysts.

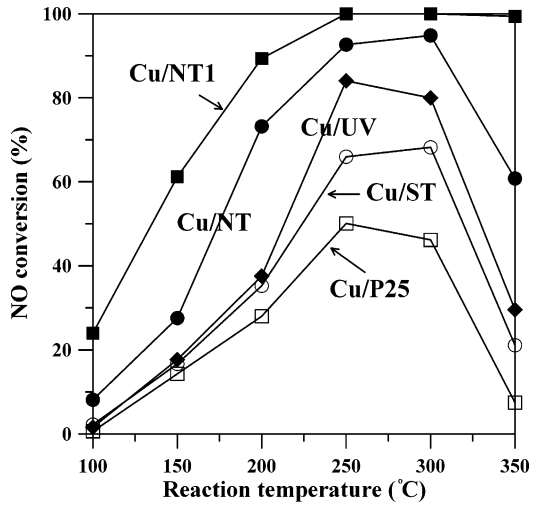

Figure 4. Variation of steady-state NO conversion with temperature for reactions over the Cu-loaded (2 wt %) TiO_2 catalysts. The reacting stream compositions: 640 ppm NO, 640 ppm NH_3, 1 vol % O_2, and He as the diluent.

the conversion drops with further increase of the temperature. The drop in NO conversion at high temperatures was attributed to the activated oxidation of NH_3 (i.e., nonselective reduction of O_2 with NH_3) to NO.[12] We have also observed a lowering of the maximum-conversion temperature by increasing Cu content beyond 2 wt %. Therefore, 2 wt % Cu/TiO_2 is the content used for the structure and activity studies to avoid a possible narrowing of the temperature window.

As to the effect of the support type, Figure 4 shows that the NO conversion over the different Cu/TiO_2 catalysts has an order of NT > UV100 > ST01. To have such a difference in conversion, there must be a significant difference in the activity of the catalysts (i.e., the specific rate or turnover frequency), especially at high conversions with reactions conducted at high temperatures. There was little difference in the crystalline phase of the TiO_2 supports. The chemical structure of the active Cu species must have played a key role determining the catalyst activity.

To analyze the structural difference of the Cu species, the catalysts were subjected to X-ray absorption fine structure spectroscopic measurements (see Supporting Information for the absorption spectra). In Figure 5a, Cu K-edge XANES spectra of CuO, Cu_2O, and Cu metal are shown. The presence of a weak feature at 8978 eV (a dipole-forbidden 1s → 3d transition)

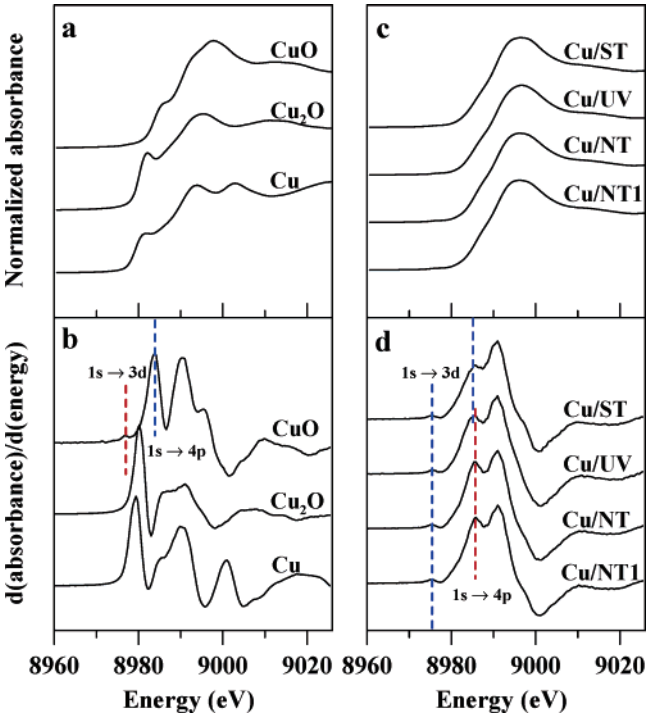

Figure 5. XANES spectra (a and c) and their first derivatives (b and d) of Cu, Cu_2O, CuO, and the Cu-loaded (2 wt %) TiO_2 catalysts.

and the lack of an intense peak below 8985 eV both are the characteristic features for the Cu^{2+} species absorption.[18−20] The dipole-allowed 1s → 4p transition for Cu^{2+} can be observed as an intense peak at ca. 8986 eV, while those for Cu^0 and Cu^{1+} can be observed at ca. 8982 and 8983 eV, respectively.[18] To make the XANES features more distinct,[19] the first derivatives of the XANES spectra have been taken and are shown in Figure 5b. The derivative spectrum of Cu^{2+} in CuO shows a more resolved 8978 eV feature for the 1s → 3d transition and a main peak, which corresponds to the edge energy for Cu^{2+} in the tetragonal symmetry, positioned at 8983.5 eV for the 1s → 4p transition. The Cu^{2+} species in the octahedral symmetry (e.g., Cu^{2+} in $Cu(OH)_2$) would have an edge energy ca. 4.5 eV larger than that of Cu^{2+} in the tetragonal symmetry.[19a] By contrast, the edge-energy features of the 1s → 4p transition for the Cu^0 and Cu^{1+} derivative spectra appear at ca. 8979 and 8980 eV, respectively (Figure 5b).

The XANES spectra of the catalysts and their first derivatives are shown in Figure 5c and d, respectively. It can be seen, especially from the derivative spectra, that the 1s → 4p transition features of Cu^0 and Cu^{1+} are not observed for all the three Cu-containing catalysts, Cu/ST, Cu/UV, and Cu/NT. Both the 1s → 3d and 1s → 4p features for Cu^{2+}, however, are present in the spectra of the catalysts, indicating that the Cu species on the catalysts are in the +2 state. A detailed inspection on the derivative spectra of CuO and the catalysts reveals that the feature for the 1s → 4p transition for the Cu^{2+} species dispersed in TiO_2 has a positive energy shift of ca. 2 eV relative to the energy for Cu^{2+} in the tetragonal symmetry (i.e., CuO). This indicates that a fraction of Cu^{2+} ions in the catalysts are in a site distorted toward the octahedral symmetry.[18c] Because Ti^{4+} in TiO_2 is in the octahedral symmetry and the bond distance of Ti−O is smaller than that of Cu−O in the CuO lattice,[19,21] it is suggested that there should be a certain amount of Cu^{2+} doped into the Ti^{4+} sites of the TiO_2 lattice for the catalysts. Furthermore, the edge energy of the tubular Cu/NT is slightly larger than those of the particulate Cu/ST and Cu/UV (Figure

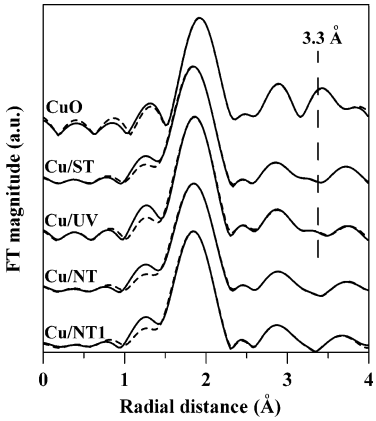

Figure 6. The Fourier transformed $k^3\chi$(k) EXAFS of the reference CuO and Cu-loaded (2 wt %) TiO_2 catalysts. The dashed line curves denote the best fitting of the EXAFS spectra.

TABLE 2: Structural Parameters, Bond Distance (*R*), and Coordination Number (CN) of CuO and TiO_2 Obtained from EXAFS Analysis[a]

catalyst	shell	*R* (Å)	CN	σ^2 (Å^2)
CuO	Cu−O	1.974	4	0.007
	Cu−O	2.781	2	0.003
	Cu−Cu	2.905	4	0.006
	Cu−Cu	3.082	4	0.006
	Cu−Cu	3.182	2	0.021
	Cu−O	3.428	2	0.007
	Cu−Cu	3.432	2	0.004
TiO_2	Ti−O	1.962	6	0.009
	Ti−Ti	3.022	4	0.009
	Ti−Ti	3.781	4	0.006
	Ti−O	3.880	8	0.001

[a] σ is the Debye−Waller factor.

5d), an indication of a higher fraction of Cu^{2+} doped into TiO_2. This aspect will be discussed further by using the EXAFS analysis.

EXAFS data for CuO, Cu_2O, and Cu metal and the catalyst samples were collected, and the normalized spectra (see Supporting Information) reveal that the local environment of the Cu ion in the catalysts resembles that in CuO, rather than that in Cu_2O or in Cu metal. The Fourier transforms (FTs) of the $k^3\chi$(k) EXAFS for the reference CuO and catalysts are shown in Figure 6, with the radial distance ranging within 4 Å. The spectra in the figure have been corrected for phase shifts. The FTs for the catalysts are somewhat different from that of CuO, especially exhibiting the lack of the strong outer-shell features possessed by the FT for CuO (see Supporting Information). As to the influence imposed by the supports, a noticeable difference is that there shows a peak at ca. 3.3 Å in the FTs of Cu/ST and Cu/UV while the tubular Cu/NT does not exhibit this feature. In pure CuO, Cu is surrounded by Cu and O ions of outer shells with bond distances near 3.3 Å (see Table 2). This difference observed for the catalysts indicates a larger grain size of CuO for the particulate Cu/ST and Cu/UV than for the tubular Cu/NT.

The bond distance (*R*) and coordination number (CN) of different shells obtained by the FEFF simulation are summarized in Table 3 for the catalysts. The fitting range for all the samples is 1−4 Å, and the bond distances given in the text and tables are phase-corrected values. Because the XANES analysis of the catalysts reflected that the chemical environment of the Cu ions is similar to that of CuO, we have used CuO as the primary model for fitting of all the catalysts. The structural parameters of CuO model compound are given in Table 2. Four coordination shells were used to fit the EXAFS data of the catalysts. The first and second shells have similar structural parameters and could be identified with Cu^{2+}−O^{2+} and Cu^{2+}−Cu^{2+} ion correlations at ca. 1.9 and 3.0 Å, respectively, although the coordination numbers are distinctly different from those in CuO. The third shells at ca. 3.3 Å could be assigned to the contribution from bonds corresponding to the Cu−Cu (3.18 Å), Cu−O (3.43 Å), and Cu−Cu (3.43 Å) coordination shells in pure CuO. However, the coordination number varies significantly with the catalyst type, showing few neighbors for Cu/NT compared to ca. two coordinated atoms for Cu/ST and Cu/UV. The fourth shell at ca. 3.8 Å cannot be accounted for using the CuO model. This suggests, on the basis of structural parameters of pure TiO_2 given in Table 2, a certain fraction of Cu^{2+} dissolved into the TiO_2 lattice, in agreement with the interpretation by the XANES analysis.

TABLE 3: Structural Parameters, Bond Distance (*R*), and Coordination Number (CN) of the Cu Species in the Cu-Loaded (2 wt %) TiO_2 Catalysts Obtained from EXAFS Analysis[a]

catalyst	shell	*R* (Å)	CN	σ^2 (Å^2)
Cu/ST	Cu−O	1.932	3.57	0.005
	Cu−Cu	2.947	5.00	0.026
	Cu−Cu	3.315	1.81	0.025
	Cu−Ti	3.837	1.36	0.009
Cu/UV	Cu−O	1.944	3.52	0.005
	Cu−Cu	3.026	4.94	0.013
	Cu−Cu	3.173	1.90	0.006
	Cu−Ti	3.802	1.40	0.015
Cu/NT	Cu−O	1.936	3.60	0.006
	Cu−Cu	3.013	5.05	0.023
	Cu−Cu	3.205	0.37	0.007
	Cu−Ti	3.807	2.01	0.017
Cu/NT1	Cu−O	1.934	3.53	0.006
	Cu−Cu	3.071	4.94	0.023
	Cu−Cu	3.296	0.29	0.004
	Cu−Ti	3.751	2.80	0.020

[a] σ is the Debye−Waller factor.

There are four-coordinated Ti−Ti at 3.78 Å (the third shell) and eight-coordinated Ti−O (the fourth shell) at 3.88 Å in pure TiO_2. These bond distances are quite close to those of the fourth shell in the catalysts. If most of the Cu^{2+} ions dissolved in TiO_2 are situated at the surface, the magnitude of third-shell Ti^{4+} and fourth-shell O^{2-} scattering should decrease because of the lower coordination number of surface sites.[18,19] Ti^{4+} on the TiO_2 surface has a coordination of 3 with third-shell Ti^{4+} and of 4 with fourth-shell O^{2-}. Therefore, Cu^{2+} ions of the catalysts stabilized in Ti^{4+} sites should have a total coordination number of 7 for the fourth shell at ca. 3.8 Å if the solid solution at surface is assumed to be in the form of $Cu_xTi_{1-x}O_2$ by assuming that the oxygen ion vacancy caused by Cu^{2+} dissolution is negligible. Taking Cu/ST as an example, the fourth shell of Cu/ST was found to contain 1.36 (Table 3) rather than the 7 ions expected for pure TiO_2 surface. This indicates that only 19% (=1.36/7) of the Cu^{2+} in the catalyst is dissolved in TiO_2, on the basis of a linear-combination principle,[18] with 81% of the Cu^{2+} in CuO or CuO-like phases. We subjected these percentage values of Cu distribution to further examination. For the first shell of the catalysts, the contribution cannot be ascribed solely to first-shell O^{2-} of CuO at 1.96 Å. Contribution from first-shell O^{2-} scattering of TiO_2 at 1.95 Å should be taken into account because of the presence of Cu^{2+} ions dissolved in TiO_2. Cu^{2+} should have a coordination number of 5 (with O^{2-}) if Cu^{2+} ions are substituted for surface Ti^{4+} in TiO_2. The first coordination of Cu^{2+} in small-size CuO or CuO-like species is 3 (O^{2-}). By adopting the preceding Cu-distribution percentages,

the first-shell coordination number of Cu/ST is calculated to have a value of 3.38 (=5 × 19% + 3 × 81%), which is close to the value obtained from the EXAFS analysis (i.e., 3.57 from Table 3).

The larger fourth-shell CN for Cu/NT than for Cu/ST and Cu/UV reflects a higher degree of Cu^{2+} dissolution into TiO_2 lattice. On the basis of the analysis for Cu distribution shown above, the percentage of Cu^{2+} dissolution in TiO_2 was found to be 20% for Cu/UV and 29% for Cu/NT. The first-shell coordination numbers calculated from these percentages, 3.40 and 3.58, respectively, for Cu/UV and Cu/NT, agree well with the EXAFS data shown in Table 3. As to the second shell of the catalysts at a distance near 3.0 Å, the contribution can be assigned, on the basis of the data in Table 2, to second-shell O^{2-} and third- and fourth-shell Cu^{2+} scattering of CuO as well as second-shell Ti^{2+} scattering of TiO_2. Because of the more multitudinous existence of possible neighbors at a distance near 3.0 Å, the larger coordination numbers observed for the second shell of the catalysts, in comparison with those for the first shell, are as expected. The third shell (at a distance of ca. 3.3 Å) of the catalysts has been ascribed to contribution from the outer shells of CuO (fifth to seventh shells). It is of interest to observe the low-degree occupancy of this shell for the nanotube-supported Cu species while Cu/ST and Cu/UV have ca. 2 coordination for this shell. This observation clearly reflects that the CuO or CuO-like clusters present on the nanotube support are much smaller in size than those supported on ST01 and UV100, thus leading to few neighbors detected at this higher coordination shell. Intercalation of Cu^{2+} into the multilayer tube wall may have prevented the agglomeration of CuO over the NT surface during calcination. The ion-exchange function of the titanate nanotubes, as a matter of fact, has been reported.[2c,9c]

The results presented above suggest the capability of the layered structure of the titanate in accommodating Cu^{2+} ions inside the layers during the course of impregnation. This leads to higher degrees of CuO dispersion and $Cu_xTi_{1-x}O_2$ formation and thus to the higher activity of the resulting catalyst. To further improve the dispersion of Cu^{2+} over the nanotubes, we employed the in-situ ion-intercalation method, in which Cu ions can intercalate into the interlayer of the titanate species during titanate nanotube formation. Under this circumstance, a large fraction of Cu^{2+} could be contained in the layered tube wall after the peeling-off of the Cu-containing layers and subsequent scrolling into tubes. After calcination, the thus-synthesized catalyst is designated as Cu/NT1. The SCR measurement was also conducted over Cu/NT1 and a very high activity, in comparison with those of the other catalysts, can be observed in Figure 4. The XANES and EXAFS spectra shown in Figures 5 and 6 reflect that the Cu species contained in Cu/NT1 is principally Cu^{2+}, a situation the same as those for the other catalysts. Similar to Cu/NT, the lack of the peak at 3.3 Å in the EXAFS reflects again a high dispersion of Cu^{2+}. The bond distance and coordination number of different shells obtained from the EXAFS simulation for Cu on Cu/NT1 are also shown in Table 3. On the basis of the Cu-distribution analysis shown above, Cu/NT1 was found to have 40% of Cu^{2+} dissolution in TiO_2. This in-situ ion-intercalation method is indeed more efficient in producing $Cu_xTi_{1-x}O_2$ solid solution for Cu supported on TiO_2. The dissolved Cu may have served as one form of the active sites for the SCR reaction,[19] thus leading to the high activity of Cu/NT1.

H_2 uptake profiles over the catalysts during temperature-programmed reduction (TPR) are shown in Figure 7. The TPR spectra show a distinct difference in the H_2-consumption pattern between the tubular and particulate catalysts. There was an obvious peak observed at ca. 320 °C for the particulate Cu/ST and Cu/UV, while the spectra of the tubular catalysts do not show the presence of peaks at temperatures above 300 °C. The H_2-consumption patterns can be decomposed into three peaks (dashed lines in Figure 7) responsible for the reduction of different Cu^{2+} species. The 320 °C peak (γ) can be assigned to reduction of bulk CuO.[19,22] For temperatures below 300 °C, the lower-temperature peak, α, can be assigned to reduction of highly dispersed CuO while the higher-temperature β peak to Cu^{2+} in the TiO_2 lattice because of metal−support interaction.[22] The negligible presence of the γ peak for Cu/NT and Cu/NT1 reflected the higher degree of Cu dispersion on the TiO_2 nanotubes than on the nanoparticles. The Cu^{2+} ions in the tubular catalysts were either situated in highly dispersed CuO or dissolved in TiO_2. The relative intensities of the β peaks were 20% for Cu/ST, 22% for Cu/UV, 28% for Cu/NT, and 42% for Cu/NT1, which were analogous to the fractions of Cu^{2+} dissolution in TiO_2 estimated by the EXAFS analysis. As to the peak temperature, the α peak for Cu/NT1 had a higher peak temperature than those for the others. This may suggest that the α-Cu^{2+} in Cu/NT1 was, as a matter of fact, situated in a transition phase between the highly dispersed CuO and TiO_2 lattice.

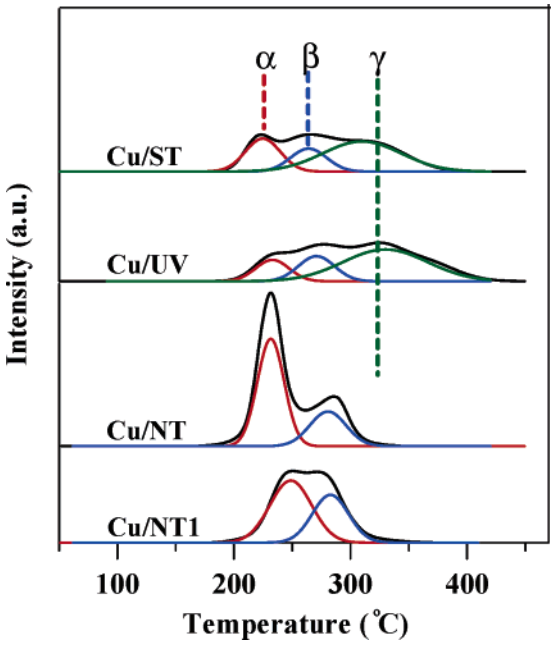

Figure 7. H_2 consumption profiles by TPR for the Cu-loaded (2 wt %) TiO_2 catalysts. Peak assignments: α for highly dispersed CuO, β for Cu^{2+} in TiO_2 lattice, and γ for bulk CuO.

The above characterizations reflected a higher degree of Cu dispersion obtained by using the titanate nanotubes as the support. The hypothetical scheme for the formation of these Cu/TiO_2 catalysts is depicted in Figure 8, in which the tube is presented as the projection along the tube axis. The intercalation of Cu^{2+} ions into the interlayer space on the tube wall may have inhibited agglomeration of the formed oxide species during calcination. To form the anatase phase, the figure shows that condensation of the titanate layers and thus rupture of the tubular framework are essential.[10f] EXAFS and TPR both reflected the negligible presence of bulk CuO species on the nanotube-supported Cu catalysts. The ion-intercalating feature of the support also promoted the dissolution of Cu^{2+} ions into the TiO_2 lattice during calcination. By contrast, the agglomeration was easier for CuO supported on nanopartices and led to the

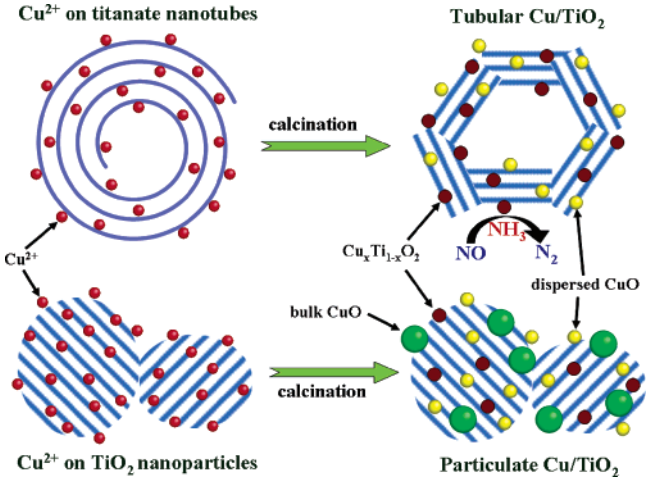

Figure 8. Scheme for the formation of the tubular and particulate Cu/TiO_2 catalysts from calcination on the Cu^{2+}-loaded supports of different structures. The $Cu_xTi_{1-x}O_2$ is considered one form of the active sites for NO reduction with NH_3.

formation of bulk CuO, as shown in Figure 8. The Cu^{2+}-substituted structure on the TiO_2 supports should be assigned one form of the active sites in the SCR because the degree of the Cu^{2+} dissolved had an order identical to that for the activity, that is, Cu/NT1 > Cu/NT > Cu/UV > Cu/ST. The in-situ ion-intercalation method to prepare Cu/NT1 was especially effective in intercalating Cu^{2+}, thus leading to the high activity of the resulting catalyst. It is expected that this tubular titanate material can be used to prepare anatase TiO_2-supported metal oxides, in addition to CuO, with a high activity in heterogeneous catalysis.

Conclusions

The present study has shown that, through intercalation of Cu^{2+} ions in the large surface-area titanate nanotubes, a high activity TiO_2-supported CuO catalyst can be obtained by calcining the Cu-loaded nanotubes. In comparison with the catalysts using TiO_2 nanoparticles as the support, the Cu species on the developed tubular Cu/TiO_2 was less prone to agglomerate under calcination and exhibited a higher activity in selective catalytic reduction of NO with NH_3. X-ray absorption analysis on the catalysts showed that the dispersion of CuO as well as the dissolution of Cu^{2+} ions into the TiO_2 lattice was promoted because of this Cu^{2+}-intercalation. The activity in the NO reduction was found to increase with the degree of Cu^{2+} dissolution, suggesting that the $Cu_xTi_{1-x}O_2$ type of solid solution should be involved in the catalytic reaction. Temperature-programmed reduction also confirmed the high degree of Cu dispersion on the tubular catalysts by showing the negligible presence of the bulk CuO. A specific feature of this tubular titanate is its structural similarity with the TiO_2 anatase. Taking advantage of this feature and the layered structure, metal ion-loaded TiO_2 catalysts with high degrees of metal-ion dispersion and solid solution formation, and thus a high activity, can be obtained.

Acknowledgment. This research is supported by the National Science Council of Taiwan (NSC 94-2214-E-006-007). We also thank Dr. Jyh-Fu Lee and Mr. Yu-Li Tai of the Taiwan Synchrotron Radiation Research Center for their help on the analysis of the XANES and EXAFS spectra.

Supporting Information Available: The TEM image of the Cu-containing tubular TiO_2; the X-ray absorption spectra, EXAFS spectra, and Fourier transformed $k^3\chi(k)$ EXAFS of Cu, Cu_2O, CuO, and Cu-loaded TiO_2 catalysts. This material is available free of charge via the Internet at http:/pubs.acs.org.

References and Notes

(1) Zanella, R.; Giorgio, S.; Henry, C. R.; Louis, C. *J. Phys. Chem. B* **2002**, *106*, 7634.

(2) (a) Hinz, A.; Larsson, P.-O.; Skåman, B.; Andersson, A. *Appl. Catal. B* **2001**, *34*, 161. (b) Perkas, N.; Wang, Y.; Koltypin, Y.; Gedanken, A.; Chandrasekaran, S. *Chem. Commun.* **2001**, *988*. (c) Bavykin, D. V.; Lapkin, A. A.; Plucinski, P. K.; Friedrich, J. M.; Walsh, F. C. *J. Catal.* **2005**, *235*, 10.

(3) (a) Long, R. Q.; Yang, R. T.; Chang, R. *Chem. Commun.* **2002**, *452*. (b) Qi, G.; Yang, R.T. *Appl. Catal. B* **2003**, *44*, 217. (c) Peña, D.A.; Uphade, B. S.; Smirniotis, P. G. *J. Catal.* **2004**, *221*, 421. (d) Popa, A. F.; Mutin, P. H.; Vioux, A.; Delahay, G.; Coq, B. *Chem. Commun.* **2004**, *2214*. (e) Ciardelli, C.; Nova, I.; Tronconi, E.; Chatterjee, D.; Bandl-Konrad, B. *Chem. Commun.* **2004**, *2718*. (f) Bourikas, K.; Fountzoula, Ch.; Kordulis, Ch. *Appl. Catal. B* **2004**, *52*, 145.

(4) (a) Komova, O. V.; Simakov, A. V.; Rogov, V. A.; Kochubei, D. I.; Odegova, G. V.; Kriventsov, V. V.; Paukshtis, E. A.; Ushakov, V. A.; Sazonova, N. N.; Nikoro, T. A. *J. Mol. Catal. A* **2000**, *161*, 191. (b) Suárez, S.; Jung, S. M.; Avila, P.; Grange, P.; Blanco, J. *Catal. Today* **2002**, *75*, 331.

(5) (a) Bond, G. C. *Heterogeneous Catalysis: Principles and Applications*; 2nd ed.; Oxford University Press: Oxford, U.K., 1987. (b) Chmielarz, L.; Kustrowski, P.; Zbroja, M.; Rafalska-Lasocha, A.; Dudek, B.; Dziembaj, R. *Appl. Catal. B* **2003**, *45*, 103.

(6) (a) Yonemitsu, M.; Tanaka, Y.; Iwamoto, M. *Chem. Mater.* **1997**, *9*, 2679. (b) Yonemitsu, M.; Tanaka, Y.; Iwamoto, M. *J. Catal.* **1998**, *178*, 207. (c) Liu, C. C.; Teng, H. *Appl. Catal. B* **2005**, *58*, 69.

(7) (a) Kasuga, T.; Hiramatsu, M.; Hoson, A.; Sekino, T.; Niihara, K. *Langmuir* **1998**, *14*, 3160. (b) Kasuga, T.; Hiramatsu, M.; Hoson, A.; Sekino, T.; Niihara, K. *Adv. Mater.* **1999**, *11*, 1307.

(8) (a) Seo, D.-S.; Lee, J.-K.; Kim, H. *J. Cryst. Growth* **2001**, *229*, 428. (b) Wang, Y. Q.; Hu, G. Q.; Duan, X. F.; Sun, H. L.; Xue, Q. K. *Chem. Phys. Lett.* **2002**, *365*, 427. (c) Yao, B. D.; Chan, Y. F.; Zhang, X. Y.; Zhang, W. F.; Yang, Z. Y.; Wang, N. *Appl. Phys. Lett.* **2003**, *82*, 281. (d) Tsai, C.-C.; Teng, H. *Chem. Mater.* **2004**, *16*, 4352. (e) Bavykin, D. V.; Parmon, V. N.; Lapkin, A. A.; Walsh, F. C. *J. Mater. Chem.* **2004**, *14*, 3370. (f) Bavykin, D. V.; Gordeev, S. N.; Moskalenko, A. V.; Lapkin, A. A.; Walsh, F. C. *J. Phys. Chem. B* **2005**, *109*, 8565. (g) Saponjic, Z. V.; Dimitrijevic, N. M.; Tiede, D. M.; Goshe, A. J.; Zuo, X.; Chen, L. X.; Barnard, A. S.; Zapol, P.; Curtiss, L.; Rajh, T. *Adv. Mater.* **2005**, *17*, 965.

(9) (a) Du, G. H.; Chen, Q.; Che, R. C.; Yuan, Z. Y.; Peng, L.-M. *Appl. Phys. Lett.* **2001**, *79*, 3702. (b) Chen, Q.; Zhou, W.; Du, G.; Peng, L.-M. *Adv. Mater.* **2002**, *14*, 1208. (c) Sun, X.; Li, Y. *Chem. Eur. J.* **2003**, *9*, 2229. (d) Zhang, S.; Peng, L.-M.; Chen, Q.; Du, G. H.; Dawson, G.; Zhou, W. Z. *Phys. Rev. Lett.* **2003**, *91*, 256103. (e) Zhu, H. Y.; Lan, Y.; Gao, X. P.; Ringer, S. P.; Zheng, Z. F.; Song, D. Y.; Zhao, J. C. *J. Am. Chem. Soc.* **2005**, *127*, 6730. (f) Pavasupree, S.; Suzuki, Y.; Yoshikawa, S.; Kawahata, R. J. *J. Solid State Chem.* **2005**, *178*, 3110. (g) Yu, H.; Yu, J.; Cheng, B.; Zhou, M. *J. Solid State Chem.* **2006**, *179*, 349. (h) Bavykin, D. V.; Friedrich, J. M.; Alexei, A.; Lapkin, A. A.; Walsh, F. C. *Chem. Mater.* **2006**, *18*, 1124. (g) Ferreira, O. P.; Souza, Filho, A. G.; Mendes, Filho, J.; Alves, O. L. *J. Braz. Chem. Soc.* **2006**, *17*, 393.

(10) (a) Yang, J.; Jin, Z.; Wang, X.; Li, W.; Zhang, J.; Zhang, S.; Guo, X.; Zhang, Z. *Dalton Trans.* **2003**, *3898*. (b) Ma, R.; Bando, Y.; Sasaki, T. *Chem. Phys. Lett.* **2003**, *380*, 577. (c) Zhang, M.; Jin, Z.; Zhang, X. G.; Yang, J.; Li, W.; Wang, X.; Zhang, Z. *J. Mol. Catal. A* **2004**, *217*, 203. (d) Ma, R.; Fukuda, K.; Sasaki, T.; Osada, M.; Bando, Y. *J. Phys. Chem. B* **2005**, *109*, 6210. (e) Tsai, C. C.; Teng, H. *Chem. Mater.* **2006**, *18*, 367. (f) Nian, J. N.; Teng, H. *J. Phys. Chem. B* **2006**, *110*, 4193.

(11) Pârvulescu, V. I.; Grange, P.; Delmon, B. *Catal. Today* **1998**, *46*, 233.

(12) (a) Jeong, S. M.; Jun, S. H.; Yoo, K. S.; Kim, S. D. *Ind. Eng. Chem. Res.* **1999**, *38*, 2210. (b) Curtin, T.; Regan, F. O.; Deconinck, C.; Knüttle, N.; Hodnett, B. K. *Catal. Today* **2000**, *55*, 189.

(13) (a) Petunchi, J. O.; Hall, W. K. *Appl. Catal. B* **1993**, *2*, L17. (b) Komatsu, T.; Ogawa, T.; Yashima, T. *J. Phys. Chem.* **1995**, *99*, 13053. (c) Cant, N. W.; Cowan, A. D. *Catal. Today* **1997**, *35*, 89. (d) Corma, A.; Fornés, V.; Palomares, E. *Appl. Catal. B* **1997**, *11*, 233. (e) Long, R. Q.; Yang, R. T. *Ind. Eng. Chem. Res.* **1999**, *38*, 873. (f) Kieger, S.; Delahay, G.; Coq, B. *Appl. Catal. B* **2000**, *25*, 1.

(14) (a) Pasel, J.; Käβner, P.; Montanari, B.; Gazzano, M.; Vaccari, A.; Makowski, W.; Lojewski, T.; Dziembaj, R.; Papp, H. *Appl. Catal. B* **1998**, *18*, 199. (b) Zhu, Z.; Liu, Z.; Liu, S.; Niu, H.; Hu, T.; Liu, T.; Xie, Y. *Appl. Catal. B* **2000**, *26*, 25. (c) Hsu, L. Y.; Teng, H. *Appl. Catal. B* **2001**, *35*, 21. (d) Teng, H.; Hsu, L. Y.; Lai, Y. C. *Environ. Sci. Technol.* **2001**, *35*, 2369. (e) Hsu, L.Y.; Teng, H. *Appl. Catal. B* **2003**, *42*, 69.

(15) Lowell, S.; Shields, J. E. *Powder Surface Area and Porosity*, 3rd ed.; Chapman & Hall: New York, 1991; pp 14−89.

(16) Stern, E. A.; Newville, M.; Ravel, B.; Yacoby, T.; Haskel, D. *Physica B* **1995**, 209, 117.

(17) (a) Powder Diffraction Files of the Joint Committee on Powder Diffraction Standards; Card No. 47-0124; International Center for Diffraction Data: Newton Square, PA, 2000. (b) Sugita, M.; Tsuji, M.; Abe, M. *Bull. Chem. Soc. Jpn.* **1990**, *63*, 1978.

(18) (a) Kau, L. S.; Spira-Solomon, D. J.; Penner-Hahn, J. E.; Hodgson, K. O.; Solomon, E. I. *J. Am. Chem. Soc.* **1987**, *109*, 6433. (b) Lu, K.; Wan, *J. Phys. Rev. B* **1987**, *35*, 4497. (c) Kau, L. S.; Hodson, K. O.; Solomon, E. I. *J. Am. Chem. Soc.* **1989**, *111*, 7103. (d) Grunet, W.; Hayes, N. W.; Joyner, R. W.; Shpiro, E. S.; Rafiq, M.; Siddigui, H.; Baeva, G. W. *J. Phys. Chem.* **1994**, *98*, 10832. (e) Kuroda, Y.; Yoshikawa, Y.; Konno, S.; Hamano, H.; Maeda, H.; Kumashiro, R.; Nagao, M. *J. Phys. Chem.* **1995**, *99*, 10621. (f) Beutel, T.; Sarkany, J.; Lei, G. D.; Yan, J. Y.; Sachtler, W. M. H. *J. Phys. Chem.* **1996**, *100*, 845.

(19) (a) Okamoto, Y.; Kubota, T.; Gotoh, H.; Ohto, Y.; Aritani, H.; Tanaka, T.; Yoshida, S. *J. Chem. Soc., Faraday Trans.* **1998**, *94*, 3743. (b) Bera, P.; Priolkar, K. R.; Sarode, P. R.; Hegde, M. S.; Emura, S.; Kumashiro, R.; Lalla, N. P. *Chem. Mater.* **2002**, *14*, 3591.

(20) (a) Huang, Y. J.; Wang, H. P. *J. Phys. Chem. A* **1999**, *103*, 6514. (b) Huang, Y. J.; Wang, H. P.; Lee, J. F. *Appl. Catal. B* **2003**, *40*, 111. (c) Liu, C. C.; Teng, H. *Appl. Catal. B* **2005**, *58*, 69.

(21) (a) Bouchet, R.; Weibel, A.; Knauth, P.; Mountjoy, G.; Chadwick, A. V. *Chem. Mater.* **2003**, *15*, 4996. (b) Zhao, L. Y.; Yang, P. C.; Wang, X. K.; Xie, Y. N.; Wu, N. Z.; Xie, Y. C. *Appl. Surf. Sci.* **2004**, *228*, 257.

(22) (a) Zhou, R. X.; Yu, T. M.; Jiang, X. Y.; Chen, F. Zheng, X. M. *Appl. Surf. Sci.* **1999**, *148*, 263. (b) Hernández-Huesca, R.; Santamaría, J.; Braos-García, P.; Maireles-Torres, P.; Rodríguez-Castellón, E.; Jiménez-López, A. *Appl. Catal. B* **2001**, *29*, 1. (c) Jiang, X. Y.; Lu, G. L.; Zhou, R. X.; Mao, J. X.; Chen, Y.; Zheng, X. M. *Appl. Surf. Sci.* **2001**, *173*, 208. (d) Chary, K. V. R.; Sagar, G. V.; Naresh, D.; Seela, K. K.; Sridhar, B. *J. Phys. Chem. B* **2005**, *109*, 9437.